Deficiency of *Rbbp1/Arid4a* and *Rbbp1l1/Arid4b* alters epigenetic modifications and suppresses an imprinting defect in the PWS/AS domain

Mei-Yi Wu,[1] Ting-Fen Tsai,[2] and Arthur L. Beaudet[1,3]

[1]Department of Molecular and Human Genetics, Baylor College of Medicine, Houston, Texas 77030, USA; [2]Department of Life Science and Institute of Genetics, National Yang-Ming University, Taipei 112, Taiwan

Prader-Willi syndrome (PWS) and Angelman syndrome (AS) are caused by deficiency of imprinted gene expression from paternal or maternal chromosome 15q11–q13, respectively. Genomic imprinting of the PWS/AS domain is regulated through a bipartite *cis*-acting imprinting center (PWS-IC/AS-IC) within and upstream of the *SNRPN* promoter. Here, we show that two Rb-binding protein-related genes, *Rbbp1*/*Arid4a* and *Rbbp1l1*/*Arid4b*, are involved in the regulation of imprinting of the IC. We recovered these two genes from gene trap mutagenesis selecting for altered expression of an *Snrpn*-EGFP fusion gene strategy. RBBP1/ARID4A is an Rb-binding protein. RBBP1/ARID4A interacts with RBBP1L1/ARID4B and with the *Snrpn* promoter, implying that both are part of a protein complex. To further elucidate their roles on regulation of imprinting, we deleted the *Rbbp1*/*Arid4a* and *Rbbp1l1*/*Arid4b* genes in mice. Combined homozygous deficiency for *Rbbp1*/*Arid4a* and heterozygous deficiency for *Rbbp1l1*/*Arid4b* altered epigenetic modifications at the PWS-IC with reduced trimethylation of histone H4K20 and H3K9 and reduced DNA methylation, changing the maternal allele toward a more paternal epigenotype. Importantly, mutations of *Rbbp1*/*Arid4a*, *Rbbp1l1*/*Arid4b*, or *Rb* suppressed an AS imprinting defect caused by a mutation at the AS-IC. These data identify *Rbbp1*/*Arid4a* and *Rbbp1l1*/*Arid4b* as new members of epigenetic complexes regulating genomic imprinting at the PWS/AS domain.

[*Keywords*: *Rbbp1*/*Arid4a*; *Rbbp1l1*/*Arid4b*; Prader-Willi/Angelman domain; genomic imprinting; epigenetic modifications]

Received May 25, 2006; revised version accepted August 28, 2006.

Genomic imprinting is regulated via *cis*-acting elements recognized by *trans*-acting factors to establish different epigenetic modifications according to the parent of origin. Prader-Willi syndrome (PWS) is caused by deficiency of an uncertain combination of protein-coding genes and snoRNAs that are expressed from paternal, but not maternal, chromosome 15q11–q13, while Angelman syndrome (AS) is caused by loss of function of the maternal allele of an E3-ubiquitin ligase (*UBE3A*) mapping within 15q11–q13 (Horsthemke and Buiting 2006). Imprinting of the PWS/AS domain is regulated through a bipartite *cis*-acting imprinting center (IC), comprised of the PWS-IC and the AS-IC within and upstream of the *SNRPN* promoter (Buiting et al. 1995, 1999; Ohta et al. 1999). The IC is marked epigenetically according to the parent of origin, which results in differential allelic expression of genes across the PWS/AS domain (Kantor et al. 2006). Allele-specific DNA methylation occurs at the PWS-IC, where the paternal allele is unmethylated and actively transcribed and the maternal allele is methylated and silent (Shemer et al. 1997; Gabriel et al. 1998). There are parent-of-origin-specific chromatin modifications of the PWS-IC domain with histone H3 Lys 9 (H3K9) methylated on the maternal allele and Lys 4 (H3K4) methylated on the paternal allele (Xin et al. 2001; Fournier et al. 2002), and with histones H3 and H4 more highly acetylated on the paternal allele than on the maternal allele (Saitoh and Wada 2000; Fulmer-Smentek and Francke 2001). In contrast, the AS-IC is modified with histone H4 acetylated and H3K4 methylated only on the maternal allele (Perk et al. 2002). Although epigenetic modifications that regulate imprinting are well defined, very little is known about epigenetic regulators that control genomic imprinting.

With the goal of screening for mutations affecting *trans*-acting factors that regulate imprinting, we combined selection for altered expression of an *Snrpn*-EGFP fusion gene with gene trap mutagenesis in mouse em-

[3]Corresponding author.
E-MAIL abeaudet@bcm.tmc.edu; FAX (713) 798-7773.
Article is online at http://www.genesdev.org/cgi/doi/10.1101/gad.1452206.

bryonic stem (ES) cells. Two gene trap clones associated with increased expression of EGFP were found to be integrations into two related *Arid* (AT-rich interaction domain) family genes, *Arid4a* and *Arid4b* (Wilsker et al. 2005), previously known as retinoblastoma-binding protein-related genes, Rb-binding protein 1 (*Rbbp1*) (Defeo-Jones et al. 1991) and *Rbbp1*-like 1 (*Rbbp1l1*) (Cao et al. 2001), respectively. This result led to studies demonstrating that *Rbbp1*/*Arid4a*, *Rbbp1l1*/*Arid4b*, and *Rb* play a role in the regulation of the PWS/AS imprinted domain, representing a novel epigenetic mechanism of regulation of genomic imprinting.

Results

ES cells expressing EGFP from the Snrpn promoter

To investigate regulation of imprinting, an EGFP gene cassette was placed in the position normally occupied by the ORF for SNRPN (Fig. 1A). *Snrpn*-EGFP ES clones were identified by Southern blot analysis using a 3′-flanking segment and EGFP as probes (Fig. 1B). The expression of the *Snrpn*-EGFP fusion gene was evaluated by flow cytometric analysis (Fig. 1C). The major peak representing 86% of targeted cells from an EGFP-neo clone expressed EGFP protein with a mean fluorescence intensity (MFI) of 6.23, while wild-type ES cells displayed a background MFI of 1.09. After the neo^r cassette was removed from the targeted allele, the percentage of EGFP-positive cells increased to 99.8%, and the MFI increased from 6.23 to 13.8.

In wild-type ES cells, the *Snrpn* promoter is unmethylated and active on the paternal allele, and is methylated and silent on the maternal allele (Shemer et al. 1997; Gabriel et al. 1998). We have reported that gene targeting at the *Snrpn* locus frequently resulted in exclusive recovery of paternal recombinants and demethylation and activation of expression for the nonrecombinant, normally silenced maternal allele (Tsai et al. 2003). This phenomenon occurred in the available *Snrpn*-EGFP ES clone with loss of methylation on the maternal allele for the *Snrpn* promoter (Fig. 1D).

Screening for variant expression of EGFP with gene trap mutagenesis

ES cells with the *Snrpn*-EGFP fusion gene were subjected to gene-trap mutagenesis using the ROSAβgeo* retroviral gene trap vector (Fig. 2A; Friedrich and Soriano 1991). After infection of 10^7 cells in each of two experiments, three clones were recovered from the population sorted for increased EGFP expression by FACS. After flow cytometric analysis, two gene trap clones (designated GT-A and GT-B) isolated from separate retroviral infection experiments had higher levels of EGFP expression (Fig. 2B). The one other clone (designated GT-C) had no

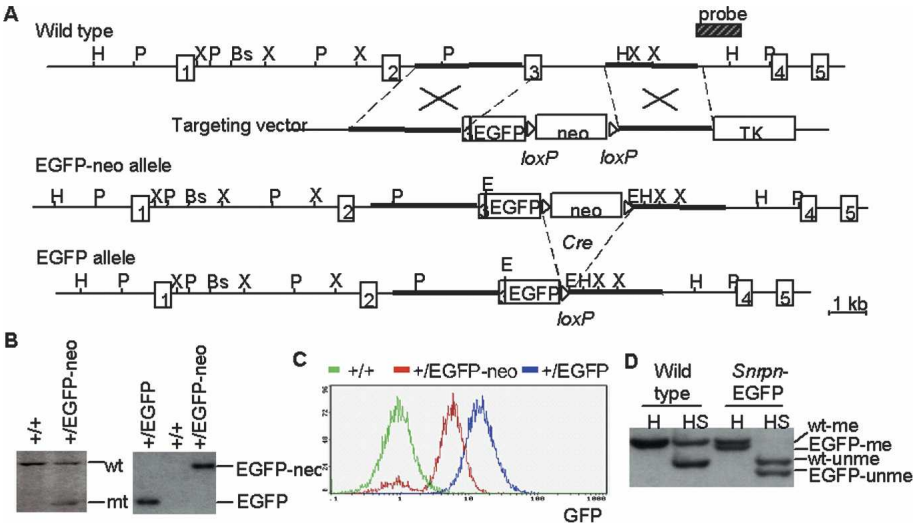

Figure 1. Generation of a *Snrpn*-EGFP fusion gene in ES cells. (*A*) Targeting strategy for constructing the *Snrpn*-EGFP fusion gene. The EGFP cassette and the neomycin resistance gene (neo) were introduced into exon 3 of *Snrpn* by homologous recombination. The neo gene, flanked by two *loxP* sites (triangles), was subsequently removed by the Cre recombinase. (TK) Herpes simplex viral thymidine kinase cassette; (H) HindIII; (P) PstI; (X) XbaI; (Bs) BssHII; (E) EcoRI. (*B*) Southern blotting analysis of wild-type (+/+) cells, the clone targeted with the EGFP-neo construct (+/EGFP-neo), and the latter cells following Cre-mediated deletion of the neo gene (+/EGFP). (*Left*) DNA was digested with PstI, and hybridized with the 3′-flanking probe shown in *A*. (Wt) The 9.0-kb fragment from the wild-type allele; (mt) the 4.3-kb fragment from the mutant EGFP-neo allele. (*Right*) DNA was digested with EcoRI and hybridized with an EGFP probe. The fragment sizes for EGFP-neo and EGFP alleles are 2.7 kb and 1.0 kb, respectively. (*C*) Flow cytometric analysis for the comparison of EGFP expression in wild-type ES cells (green), the EGFP fusion gene with neo present (red), and the EGFP clone with neo deleted (blue). The scale is cell number on the *left* and relative fluorescence *below*. (*D*) Methylation analysis of the *Snrpn* CpG island in the *Snrpn*-EGFP clone. Genomic DNA was digested with HindIII (H) alone or in combination with SacII (HS) for Southern blot analysis. (Wt-me) The 14-kb methylated DNA; (wt-unme) the 10.2-kb unmethylated DNA from the wild-type *Snrpn* allele; (EGFP-me) the 13.2-kb methylated DNA; (EGFP-unme) the 9.4-kb unmethylated DNA from the *Snrpn*-EGFP fusion allele.

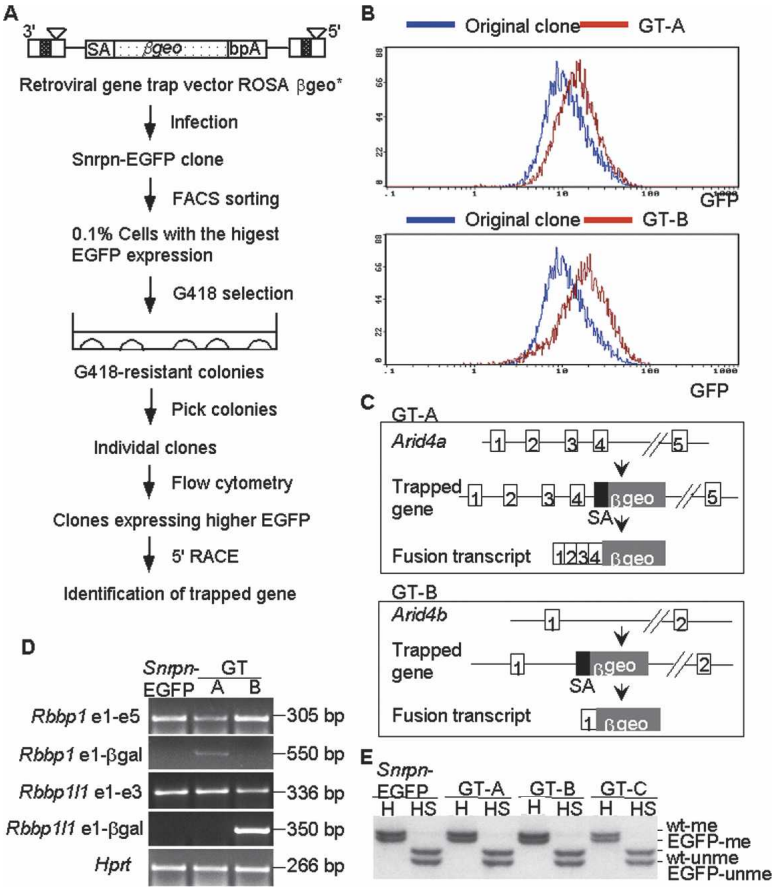

Figure 2. Gene trap mutagenesis using the *Snrpn*-EGFP fusion clone. (*A*) Scheme for screening mutagenized cells. A retroviral vector, ROSAβgeo*, was used to infect the *Snrpn*-EGFP clone. The infected cells were sorted by FACS, and the 0.1% of cells with the highest EGFP expression were plated onto the feeder cell plates and selected with G418. The G418-resistant colonies were picked, and the level of EGFP expression for individual clones was confirmed by flow cytometric analysis. Then, identification of the trapped gene was achieved by 5′-RACE. (SA) Splice acceptor site; (βgeo) a fusion reporter gene including β-galactosidase and neomycin resistance activities. (*B*) Flow cytometric analysis for the comparison of the original *Snrpn*-EGFP clone (original clone) with the GT-A (*top*) and GT-B (*bottom*) clones. (*C*) Schematic representations of the trapped genes. (*D*) Expression analysis of *Arid4a*, *Arid4b*, and their transcripts fused with βgeo by RT–PCR. "e" refers to exon number, as in e1 for exon 1. (*E*) Methylation analysis of the *Snrpn* CpG island in the original *Snrpn*-EGFP clone and three gene trap clones. Southern blot analysis is similar to Figure 1D.

change in the level of EGFP expression compared with the original *Snrpn*-EGFP clone (data not shown). The GT-A clone had an MFI of 17, and the GT-B clone had an MFI of 22, while the control *Snrpn*-EGFP ES cells had an MFI of 13. Sequencing of the trapped genes for the GT-A and GT-B clones resulted in the identification of two related *Arid* family genes, *Arid4a* and *Arid4b* (Wilsker et al. 2005), previously known as Rb-binding protein-related genes, *Rbbp1* (Defeo-Jones et al. 1991) and *Rbbp1l1* (Cao et al. 2001), respectively. Comparison of the fusion cDNA and genomic DNA sequences predicted that insertion of the gene trap vector occurred between exons 4 and 5 for *Arid4a* in the GT-A clone and within intron 1 for *Arid4b* in the GT-B clone (Fig. 2C). RT–PCR analysis showed reduction in the transcripts for *Arid4a* and *Arid4b* in the GT-A and GT-B clones, respectively (Fig. 2D). Fusion transcripts were detected with the first four exons of *Arid4a* linked to the geo sequence in the GT-A clone and with exon 1 of *Arid4b* linked to the geo sequence in the GT-B clone (Fig. 2D). These results indicated that insertion of the gene trap vector into *Arid4a* or *Arid4b* led to increased expression of the *Snrpn*-EGFP fusion gene, although the *Snrpn* promoter on the fusion allele was unmethylated and already actively transcribed in the original *Snrpn*-EGFP and GT clones (Figs. 1C,D, 2E). This "superactivation" might be due to changes of other epigenetic effects, such as chromatin modifications.

Interaction of ARID4A with ARID4B and the Snrpn promoter

Having identified two homologous genes, *Arid4a* and *Arid4b*, we tested for protein interactions between ARID4A and ARID4B (Fig. 3A). Coimmunoprecipitation experiments combined with Western blot analysis showed that V5-tagged mouse ARID4B was associated with Flag-tagged human ARID4A (Fig. 3B, top) and with endogenous human ARID4A (Fig. 3B, bottom) in human embryonic kidney 293 cells. To examine whether ARID4A interacts with the *Snrpn* promoter that was used to drive EGFP expression in the gene trap mutagenesis screen, we performed chromatin immunoprecipitation (ChIP) analysis (Fig. 3C). We found that DNA at −6704, −4750, −2626, and +44 of the *Snrpn* promoter was associated with ARID4A, whereas DNA at +1238, exon 3, and exon 7 of the *Snrpn* gene was not. Taken together, the data demonstrated the interaction of ARID4A with ARID4B and with the *Snrpn* promoter.

Generation of mice with the Arid4a and Arid4b deletions

In order to evaluate the function of *Arid4a* and *Arid4b* in mice, both gene loci were independently deleted by homologous recombination in ES cells (Fig. 4A,E). The tar-

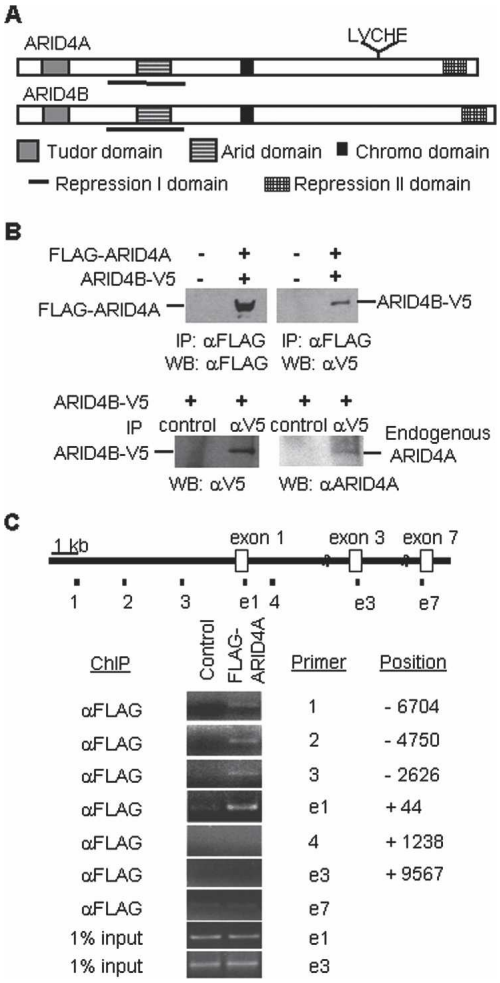

Figure 3. Interaction of ARID4A with ARID4B and with the *Snrpn* promoter. (*A*) Comparison of ARID4A and ARID4B. (*B*) Association between ARID4A and ARID4B. (*Top*) Expression vectors for Flag-ARID4A and ARID4B-V5 were cotransfected into 293 cells. Immunoprecipitation was performed with anti-Flag antibody. Total ARID4A and coimmunoprecipitated ARID4B were detected by Western blot assays using anti-Flag antibody (*left*) and anti-V5 antibody (*right*), respectively. (*Bottom*) 293 cells were transfected with the ARID4B-V5 vector. Immunoprecipitation was performed with anti-V5 antibody and normal mouse IgG as a control antibody. Total ARID4B and coimmunoprecipitated cell-endogenous ARID4A were detected by anti-V5 antibody (*left*) and an antibody for ARID4A (*right*), respectively. (*C*) ChIP analysis for ARID4A in the *Snrpn* promoter region. (*Top*) The *Snrpn* promoter region is shown with bars to indicate the amplified region of each PCR product used in the ChIP analysis. The amplified products from primer sets of 1, 2, 3, e1, and 4 were within or near the *Snrpn* promoter. Primer sets e1, e3, and e7 overlap the exons of the respective numbers. (*Bottom*) Cross-linked chromatin was immunoprecipitated with anti-Flag antibody from wild-type ES cells (control) or the ES clone stably expressing Flag-tagged ARID4A. DNA from immunoprecipitated chromatin or cell extracts (1% input) was subjected to PCR for the sites shown *above*.

geted ES cell clones were identified by Southern blotting and PCR analysis (Fig. 4B,F) and were used to generate chimeric mice that transmitted the mutated *Arid4a* or *Arid4b* alleles to the mouse germline. Mice heterozygous (+/–) or homozygous (–/–) for *Arid4a* deficiency were viable and fertile. The deleted allele was verified by Southern blotting (Fig. 4C), and absence of the transcripts was confirmed by RT–PCR (Fig. 4D). In contrast, *Arid4b*$^{-/-}$ mice were not born alive, although *Arid4b*$^{+/-}$ mice were viable and fertile (Table 1). We examined embryos from timed matings between heterozygotes, and did not find any *Arid4b*$^{-/-}$ embryos from embryonic days 7.5–13.5 (E7.5–E13.5). At E3.5, we found that two out of 12 blastocysts from two different intercrosses were homozygous for the *Arid4b* mutation (Fig. 4G; Table 1). These data suggested that embryonic demise occurs between E3.5 and E7.5.

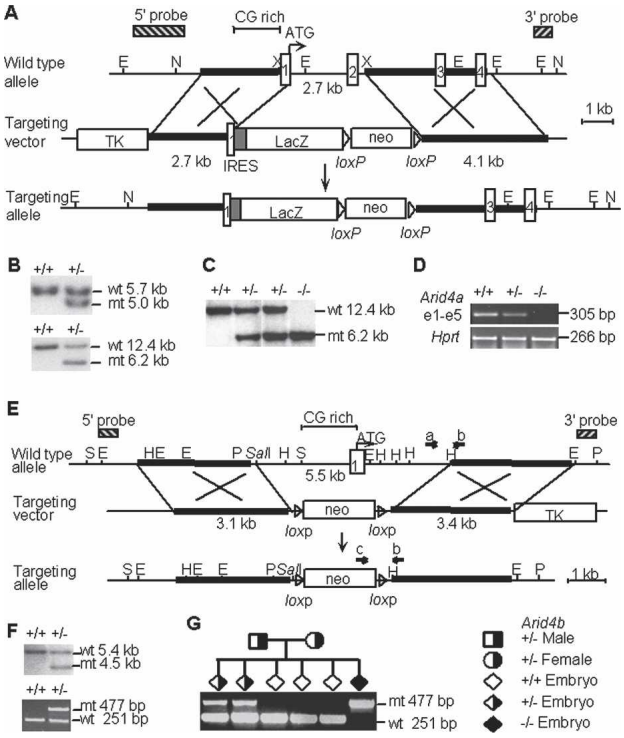

Figure 4. Targeted disruption of the *Arid4a* and *Arid4b* genes. (*A*) Targeting strategy for disrupting the *Arid4a* gene in ES cells. (IRES) Internal ribosome entry site; (TK) herpes simplex viral thymidine kinase cassette; (E) EcoRI; (N) NcoI; (X) XhoI. (*B*) Southern blot analysis of the *Arid4a* targeted ES clone using the 5′-flanking probe (*top*) and the 3′-flanking probe (*bottom*). (Wt) Wild-type allele; (mt) mutant allele. (*C*) Southern blotting using the 3′-flanking probe for genotype analysis of offspring from the *Arid4a*$^{+/-}$ mice intercross. (*D*) RT–PCR analysis for *Arid4a* expression using primer pairs in exons 1 and 5 (e1-e5) in wild-type, *Arid4a*$^{+/-}$, or *Arid4a*$^{-/-}$ mice. (*E*) Targeting strategy for disrupting the *Arid4b* gene in ES cells. Horizontal bold arrows (a, b, and c) indicate the positions of primers used to assay genotype in *F*; primers a and b amplify the wild-type allele, and b and c amplify the mutant allele. (S) SstI; (E) EcoRI; (H) HindIII; (P) PstI. (*F*) Genotype analysis of the *Arid4b*-targeted ES clone by Southern blotting using the 5′-flanking probe (*top*) and by PCR using the primers shown in *E* (*bottom*). (*G*) Genotype identification of a litter of six E3.5 embryos from mating between *Arid4b*$^{+/-}$ heterozygotes by PCR as in *F*.

Table 1. *Analysis of progeny from intercrosses of* Arid4b$^{+/-}$ *mice*

Mice	Total number	Mouse genotypes		
		Arid4b$^{+/+}$	*Arid4b*$^{+/-}$	*Arid4b*$^{-/-}$
8 wk	108	39	69	0

Gestational stages	Embryos	Reabsorptions	Embryo genotypes		
			Arid4b$^{+/+}$	*Arid4b*$^{+/-}$	*Arid4b*$^{-/-}$
E13.5	7	3	4	3	0
E10.5	7	2	3	4	0
E7.5	21	7	10	11	0
E3.5	12	0	5	5	2

Deficiency of Arid4a and Arid4b alters epigenetic modifications at the PWS-IC

The trapping of the *Arid4a* and *Arid4b* genes led us to assess their function in the regulation of imprinting for the PWS/AS region. To determine whether the *Arid4a* or *Arid4b* mutation was accompanied by any imprinting defect, we examined the epigenetic status of the PWS-IC located at the *Snrpn* promoter, beginning with DNA methylation. Both *Arid4a*$^{-/-}$ mice and *Arid4b*$^{+/-}$ mice displayed normal differential DNA methylation at the *Snrpn* promoter (data not shown). Therefore, we intercrossed *Arid4a*$^{-/-}$ mice and *Arid4b*$^{+/-}$ mice to produce *Arid4a*$^{+/-}$ *Arid4b*$^{+/-}$ mice. The double-heterozygous mice were then used to derive mice with triallelic mutations (*Arid4a*$^{-/-}$ *Arid4b*$^{+/-}$), since double-null mutations (*Arid4a*$^{-/-}$ *Arid4b*$^{-/-}$) were not viable. By Southern blot analysis using the methylation-sensitive SacII enzyme, one out of seven *Arid4a*$^{-/-}$ *Arid4b*$^{+/-}$ mice showed loss of DNA methylation (Fig. 5A, mouse 5); in contrast, the other six *Arid4a*$^{-/-}$ *Arid4b*$^{+/-}$ mice displayed differential methylation patterns similar to those of wild-type mice (Fig. 5A). Use of bisulfite sequencing to analyze 16 CpGs at exon 1 of *Snrpn* showed a variable pattern of hypomethylation in the *Arid4a*$^{-/-}$ *Arid4b*$^{+/-}$ mice (Fig. 5B). In mutant mice 1 and 2, there were no significant changes in the methylation pattern compared with wild-type mice. In mutant mice 3 and 4, the *Snrpn* CpGs were less methylated than those in wild-type controls. In mutant mouse 5, both parental chromosomes were unmethylated, which confirmed the lack of methylation shown in Southern blot analysis. We have analyzed a similar number of wild-type littermates that all have normal methylation patterns at *Snrpn* by Southern blotting and bisulfite sequencing analysis (data not shown).

We next examined histone modifications at the PWS-IC using ChIP analysis. The *Arid4a*$^{-/-}$ *Arid4b*$^{+/-}$ mice showed a variable decrease in trimethylation of H3K9 (Fig. 5C). While mutant mouse 1, which was associated with a normal DNA methylation pattern at *Snrpn*, showed a slight reduction, mutant mouse 5, which was accompanied by lack of DNA methylation at *Snrpn*, had a marked reduction in H3K9 trimethylation. Notably, there was a significant decrease in trimethylation of H4K20 in all of the *Arid4a*$^{-/-}$ *Arid4b*$^{+/-}$ mice (Fig. 5C, mutant mice 1 and 5; data not shown for mutant mice 2–4). These results suggested that *Arid4a* and *Arid4b* have a major role in controlling H4K20 trimethylation, although it is possible that the alterations in H3K9 trimethylation and DNA methylation patterns are intimately linked with altered H4K20 trimethylation.

Trimethylated H3K9 and H4K20 are marks of repressive chromatin states (Bannister and Kouzarides 2005). In the promoter region of human *SNRPN*, H3K9 is more methylated on the maternal allele than the paternal allele (Xin et al. 2001). We examined allelic differential modifications for H3K9 and H4K20 trimethylation using mice with a 4.8-kb deletion at *Snrpn* exon 1 (Bressler et al. 2001), the equivalent of a human PWS-IC deletion. ChIP analysis showed that the maternal copy of the *Snrpn* promoter was modified with both H3K9 and H4K20 trimethylation, which was present in mice with the paternal 4.8-kb deletion (Δ4.8 m+/p–), whereas there was dramatic reduction of both modifications on the paternal copy, which was present in mice inheriting the 4.8-kb deletion maternally (Δ4.8 m–/p+) (Fig. 5D). Taken together, these results indicate that *Arid4a* and *Arid4b* play a role in controlling maternal-specific H4K20 and H3K9 trimethylation and DNA methylation at the PWS-IC with the maternal allele in the *Arid4a*$^{-/-}$ *Arid4b*$^{+/-}$ mice being changed toward a more paternal epigenotype.

We next determined whether the observed acquisition of the paternal epigenotype at the PWS-IC on the maternal chromosome was correlated with increased expression of paternally expressed genes and decreased expression of maternally expressed genes in the PWS/AS region. Quantitative RT–PCR analysis demonstrated a 1.7-fold increased abundance of *Snrpn* transcripts in the *Arid4a*$^{-/-}$ *Arid4b*$^{+/-}$ mice compared with wild-type mice (Fig. 5E). A similar result was found for another paternally expressed gene, necdin (*Ndn*), with a 1.8-fold increased abundance of mRNA (Fig. 5E). In contrast, Western blot analysis showed a slight decrease in E6-AP encoded by the maternally expressed gene *Ube3a* in the *Arid4a*$^{-/-}$ *Arid4b*$^{+/-}$ mice when compared with wild-type mice (Fig. 5F).

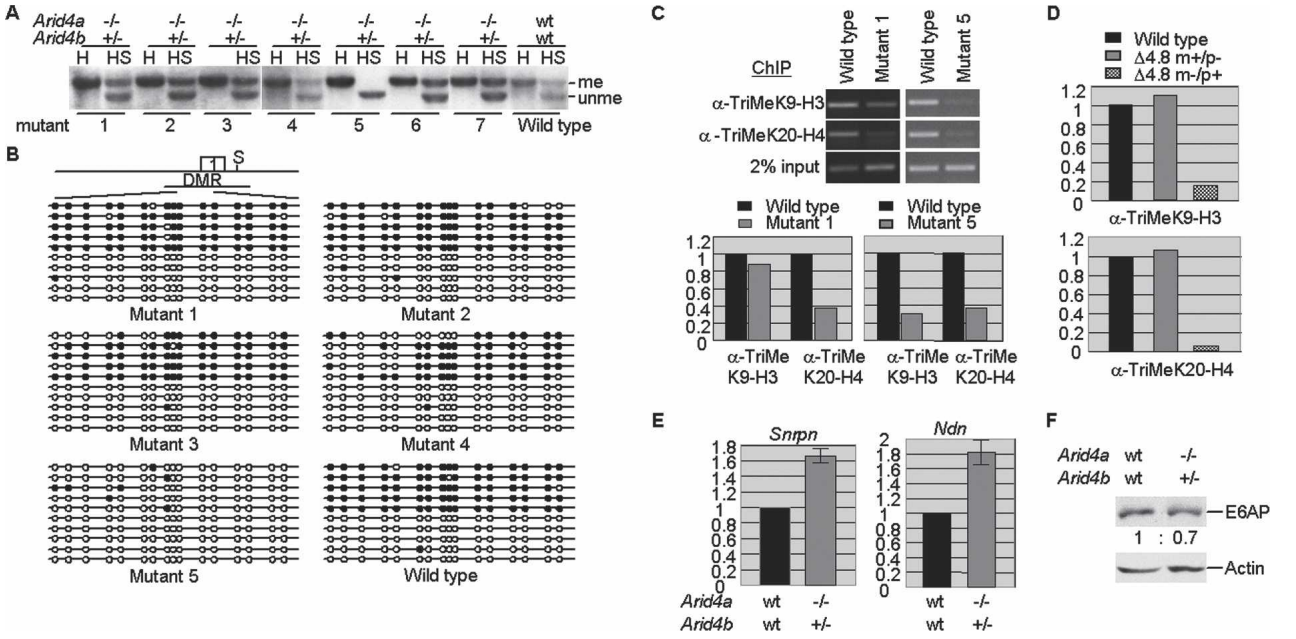

Figure 5. Epigenetic analysis of the PWS-IC in *Arid4a*$^{-/-}$ *Arid4b*$^{+/-}$ mice. (*A*) Southern blot analysis for DNA methylation at the *Snrpn* CpG island. Genomic DNA isolated from seven *Arid4a*$^{-/-}$ *Arid4b*$^{+/-}$ mice and one wild-type control was digested with HindIII (H) alone or in combination with SacII (HS) for Southern blot analysis. (Me) The 14-kb methylated DNA; (unme) the 10.2-kb unmethylated DNA from the *Snrpn* allele. (*B*) Bisulfite sequence analysis of methylation status of 16 CpG dinucleotides across the exon 1 region (–307 to +115) of *Snrpn* in wild-type mice and *Arid4a*$^{-/-}$ *Arid4b*$^{+/-}$ mice (mutant mice 1–5). Each line represents an individual clone with open and closed circles corresponding to unmethylated and methylated CpGs, respectively. (S) A SacII site; (DMR) differential methylation region. (*C*) ChIP analysis for H3K9 and H4K20 trimethylation at the *Snrpn* promoter in the *Arid4a*$^{-/-}$ *Arid4b*$^{+/-}$ mice (mutant mice 1 and 5). (*Top*) DNA isolated from immunoprecipitated chromatin using anti-trimethylated H3K9 or anti-trimethylated H4K20 antibodies and from cell crude extracts (2% input) was subjected to PCR using the primer pair e1 shown in Figure 3C. (*Bottom*) Quantification of trimethylated H3K9 and trimethylated H4K20 by real-time PCR analysis. (*D*) ChIP analysis for wild-type mice, mice paternally inheriting the 4.8-kb deletion (Δ4.8 m+/p–), or mice maternally inheriting the 4.8-kb deletion (Δ4.8 m–/p+) using anti-trimethylated H3K9 (*top*) or anti-trimethylated H4K20 (*bottom*) antibodies. Quantification of trimethylated H3K9 and trimethylated H4K20 in the *Snrpn* promoter region was assayed by real-time PCR using the primer pair e1 shown in Figure 3C. (*E*) Quantitative RT–PCR analysis for two paternally expressed genes, *Snrpn* (*left*) and *Ndn* (*right*), in wild-type mice and the *Arid4a*$^{-/-}$ *Arid4b*$^{+/-}$ mice. The level of gene expression measured for the wild-type mice was set as 1. (*F*) Western blot analysis for maternally expressed gene *Ube3a* using an antibody to E6-AP or a control antibody to actin. Ratios of expression were quantitated by densitometry. The level of E6-AP was normalized against actin level for each sample. The level of *Ube3a* expression measured for the wild-type mouse was set as 1.

Mutations of Arid4a, Arid4b, or Rb suppressed an AS-IC imprinting defect

Although a murine equivalent to the human AS-IC has not yet been identified, we have recently reported a mouse model of an AS imprinting defect with the AS-IC^{an} mutation (Wu et al. 2006). To further investigate the roles of *Arid4a* and *Arid4b* in the regulation of imprinting for the PWS/AS region, we examined the genetic interaction of these two genes with the AS-IC by mating female mice with the AS-IC^{an} mutation to male mice carrying the *Arid4a* or *Arid4b* mutations (Fig. 6). Using DNA derived from the offspring for methylation analysis of the *Snrpn* and *Ndn* CpG islands by Southern blotting, mice inheriting only the AS-IC^{an} mutation had an absence of methylation on both alleles for *Snrpn* and reduced methylation of DNA at the *Ndn* locus (Fig. 6A, mouse 5) as previously reported (Wu et al. 2006). Interestingly, transmission of both the AS-IC^{an} and *Arid4b* mutations to double-heterozygous offspring demonstrated an approximately equal intensity of methylated and unmethylated fragments at *Snrpn* and *Ndn* CpG islands (Fig. 6A, mice 3 and 4), which was similar to the results for wild-type littermates (Fig. 6A, mouse 1) and for mice carrying only the *Arid4b* mutation (Fig. 6A, mouse 2). Data from additional litters showed that progeny inheriting only the AS-IC^{an} mutation displayed a complete absence of methylation at *Snrpn*, and progeny inheriting both *Arid4b* and AS-IC^{an} mutations fell into two clear methylation patterns (Fig. 6B). Five out of 12 double-heterozygous mice had the normal differential methylation pattern, while seven double-heterozygous mice showed a lack of methylation. Similar results were observed in the offspring from the mating of male mice carrying the *Arid4a* deletion to female mice with an AS-IC^{an} mutation (Fig. 6C). Four out of 18 double-heterozygous progeny showed normal differential methylation. Since *Arid4a* is an *Rb*-binding protein (Defeo-Jones et al. 1991), we mated female mice with an AS-IC^{an} mutation to male mice carrying an *Rb*-null mutation (Fig. 6D; Lee

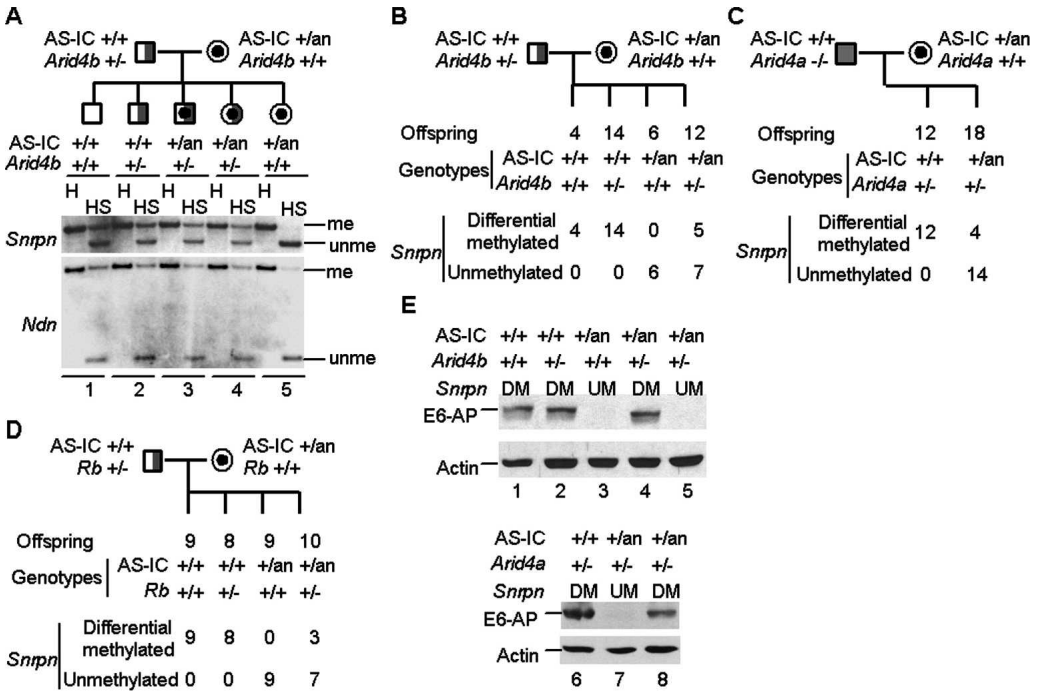

Figure 6. Suppression of an AS-IC imprinting defect by the *Arid4a* and *Arid4b* mutations. (*A*) Southern blot analysis for methylation patterns at the *Snrpn* and *Ndn* CpG islands in progeny from mating a female bearing the AS-IC^{an} mutation to a male carrying the *Arid4b* mutation. Genomic DNA was digested with HindIII (H) alone or in combination with SacII (HS) and hybridized with a probe from *Snrpn* intron 1 (*top*) or from the *Ndn* 5′-flanking region (*bottom*). Fragment sizes for the *Snrpn* CpG island: me, 14 kb; unme, 10.2 kb. Fragment sizes for the *Ndn* CpG island: me, 3.4 kb; unme, 1.9 kb. (me) Methylated; (unme) unmethylated. (*B–D*) Summary of methylation status at *Snrpn* in progeny with all genotypes from mating female mice bearing the AS-IC^{an} mutation to male mice carrying the *Arid4b*$^{+/-}$ (*B*), *Arid4a* $^{-/-}$ (*C*), or *Rb*$^{+/-}$ (*D*) mutations. (*E*) Expression analysis for *Ube3a*. Protein was extracted from the cerebral cortex of mice with different mutation combinations accompanied by either differential methylation (DM) or fully unmethylated (UM) at *Snrpn*. Western blot analysis was performed using an antibody to E6-AP or to actin.

et al. 1992). Three out of 10 mice heterozygous for both the AS-IC^{an} and *Rb* mutations had the corrected differential methylation pattern. These results indicated that haploinsufficiency for *Arid4a*, *Arid4b*, or *Rb* suppressed the imprinting defect in a fraction of mice with the AS-IC^{an} mutation. In all cases, the suppression of the imprinting defect must occur after fertilization, since the two mutations are not together until that time.

In the second generation, female mice carrying both AS-IC^{an} and *Arid4a* mutations but showing no suppression of the AS imprinting defect (lack of methylation at *Snrpn*) were mated to *Arid4a*$^{-/-}$ male mice (Fig. 7A). Surprisingly, all progeny with the AS-IC^{an} mutation showed suppression of the imprinting defect (i.e., normal differential methylation at *Snrpn*) whether homozygous or heterozygous for the *Arid4a* mutation. This result indicated complete suppression of the AS imprinting defect when both parents carry the *Arid4a* mutation. If wild-type male mice were mated to female mice carrying both AS-IC^{an} and *Arid4a* mutations with no suppression of the imprinting defect, progeny inheriting the AS-IC^{an} mutation did not show suppression either (Fig. 7B). On the other hand, when wild-type male mice were mated to female mice carrying both mutations accompanied by corrected differential methylation at *Snrpn*, all progeny with the AS-IC^{an} mutation showed a normal differential methylation pattern (Fig. 7C). This result suggested epigenetic inheritance of suppression of the AS-IC imprinting defect.

The maternally expressed Angelman gene, *Ube3a*, has been shown to be repressed in the AS-IC^{an} mutants (Wu et al. 2006). We examined *Ube3a* expression in mice carrying the AS-IC^{an} mutation together with *Arid4a* or *Arid4b* mutations (Fig. 6E). Using Western blotting to analyze E6-AP encoded by the *Ube3a* gene, double-heterozygous mice with the imprinting defect (absence of methylation at *Snrpn* as in mouse 5 for AS-IC^{an} *Arid4b*$^{+/-}$ and mouse 7 for AS-IC^{an} *Arid4a*$^{+/-}$) showed a severe decrease in E6-AP, which was similar to the result shown for mice inheriting only the AS-IC^{an} mutation (mouse 3). In contrast, double-heterozygous mice with suppression of the imprinting defect (normal differential methylation pattern at *Snrpn* as in mouse 4 for AS-IC^{an} *Arid4b*$^{+/-}$ and mouse 8 for AS-IC^{an} *Arid4a*$^{+/-}$) showed a level of protein comparable to that found in wild-type mice, *Arid4a*$^{+/-}$ mice, or *Arid4b*$^{+/-}$mice (Fig. 6E, mice 1, 6, and 2, respectively). These results indicated that *Arid4a* and *Arid4b* mutations suppressed the repression of *Ube3a* caused by the AS-IC^{an} mutation. This suppression was correlated with the correction of the differential methylation pattern at *Snrpn*.

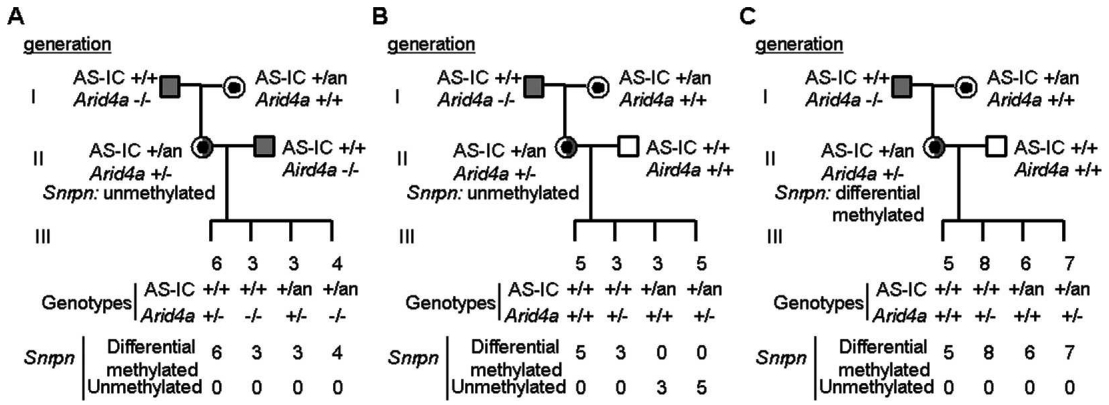

Figure 7. Completed suppression of the AS-IC imprinting defect. In the first generation, female mice with the AS-IC^{an} mutation were mated to male mice homozygous for the *Arid4a* mutation. In the second generation, double-heterozygous females with a lack of methylation at *Snrpn* were mated to *Arid4a*$^{-/-}$ males (*A*) and wild-type males (*B*), or double-heterozygous females with differential methylation at *Snrpn* were mated to wild-type males (*C*). The methylation status of *Snrpn* was analyzed in progeny with all four genotypes in the third generation.

Discussion

Both ARID4A and ARID4B contain three conserved domains: a Tudor domain, an ARID domain, and a chromodomain (Wilsker et al. 2005), as well as two repression domains—repression I and II (Fig. 3A; Lai et al. 1999a). A part of the repression I domain overlaps the Arid domain. The ARID domain contains a helix–turn–helix structure with DNA-binding activity (Patsialou et al. 2005). Chromodomains, as well as Tudor domains, mediate binding to methylated histones H3 and H4 (Bannister and Kouzarides 2005). For example, the chromodomain of heterochromatin protein 1 (HP1) binds to methylated H3K9 (Bannister et al. 2001; Lachner et al. 2001), and the Tudor domain of Cut5-repeat-binding protein 2 recognizes methylated H4K20 (Sanders et al. 2004). Both ARID4A and ARID4B have been reported to be associated with the mSIN3-histone deacetylase complex (Lai et al. 2001; Fleischer et al. 2003). The ARID4A sequence, but not ARID4B, contains a LVCHE sequence as a conserved LXCXE motif known to interact with RB (Fig. 3A). ARID4A has been defined as a repressor of E2F transcription recruited by RB (Lai et al. 1999a,b, 2001). In the past few years, there is growing evidence that RB is a component of chromatin-remodeling complexes that mediate repression of transcription (Zhu 2005). RB is necessary to direct H3K9 methylation and HP1 to promoters (Nielsen et al. 2001). In addition, the RB family maintains trimethylation of H4K20 at constitutive heterochromatin (Gonzalo et al. 2005). Here, we show that *Arid4a* and *Arid4b* participate in chromatin modifications affecting H4K20 and H3K9 trimethylation at the PWS-IC. Our analysis of the *Arid4a* and *Arid4b* deletion mice for epigenetic alterations at the PWS-IC and for suppression of the AS-IC imprinting defect suggests an in vivo function of *Arid4a* and *Arid4b* on the regulation for the PWS/AS domain. The effects could be through direct interaction of ARID4A and ARID4B with chromatin complexes binding to PWS-IC or AS-IC, or it might occur through intermediate steps involving various pathways that are modulated through chromatin remodeling.

There are seemingly opposite effects of *Arid4a/4b* deficiency on DNA methylation at the PWS-IC with decreased methylation in mice with a wild-type PWS/AS domain compared with increased methylation in mice with the AS-IC mutation. On the AS-IC and PWS-IC, there are opposite parent-of-origin-specific chromatin modifications. The PWS-IC domain on the paternal allele is associated with active chromatin modifications with Lys 4 (H3K4) methylated (Xin et al. 2001; Fournier et al. 2002), and with histones H3 and H4 more highly acetylated (Saitoh and Wada 2000; Fulmer-Smentek and Francke 2001). On the maternal allele, the PWS-IC is modified with repressive chromatin states, such as H4K20 and H3K9 trimethylation (Fig. 5D). In contrast, the human AS-IC on the maternal allele is associated with active chromatin modifications with histone H4 acetylated and H3K4 methylated (Perk et al. 2002). Deficiency of *Arid4a* and *Arid4b* in mice with a wild-type PWS/AS domain changed the repressive chromatin modifications to the active states at the PWS-IC on the maternal allele with a significant decrease in trimethylation of histone H4K20 in all of the *Arid4a*$^{-/-}$ *Arid4b*$^{+/-}$ mice, and with partially reduced H3K9 trimethylation and DNA methylation (Fig. 5). It is possible that the alterations in H3K9 trimethylation and DNA methylation patterns are intimately linked with altered H4K20 trimethylation. On the other hand, in the mouse model of an AS imprinting defect with the AS-IC^{an} mutation (Wu et al. 2006), the active chromatin modifications on the AS-IC of the maternal allele may become repressive due to the insertion of the targeting vector, which caused loss of methylation at the *Snrpn* promoter. *Arid4a*, *Arid4b*, or *Rb* mutations might shift the abnormal repressive histone modifications to a more active state at the AS-IC. Therefore, the imprinting defect with the AS-IC^{an} mutation could be suppressed and the *Snrpn* promoter on the maternal allele could turn to be normally

methylated. Taken together, *Arid4a*, *Arid4b*, and *Rb* might have a major role in shifting repressive histone modifications toward a more active state at both the PWS-IC and the AS-IC. The apparent opposite effects of deficiency of *Arid4a* and *Arid4b* on DNA methylation at the *Snrpn* promoter involve two different genotypes at the PWS/AS domain; we observed decreased DNA methylation in the *Arid4a*$^{-/-}$ *Arid4b*$^{+/-}$ mice with the wild-type PWS/AS domain (Fig. 5), and gain of DNA methylation in the AS-IC^{an} mice together with the *Arid4a*, *Arid4b*, or *Rb* mutations (Figs. 6, 7). In both cases, we believe that deficiency of *Arid4a* and *Arid4b* is shifting chromatin from a more repressed to a more active state, in one case acting at the wild-type PWS-IC and in the other case acting through the mutant AS-IC. Loss or gain of DNA methylation could be the secondary consequences linked with the chromatin states, since histone modifications have been considered to play a dominant role in the cytosine methylation (Quina et al. 2006). In ES cells, deficiency of *Arid4a* or *Arid4b* leads to superactivation of the *Snrpn*-EGFP fusion allele (Fig. 2B), in which the *Snrpn* promoter was unmethylated and already actively transcribed in the original *Snrpn*-EGFP and GT clones (Figs. 1C,D, 2E). This superactivation might be due to changes of the chromatin modifications. The chromatins, although active, may be pushed into an even more active configuration.

Mice with the AS-IC^{an} mutation represent a model system for the imprinting defect form of Angelman syndrome (Wu et al. 2006). The AS-IC mutation showed an imprinting defect with lack of methylation at the maternal *Snrpn* promoter and decreased expression of maternally expressed Angelman genes, *Ube3a*. In this paper, we showed that the suppression of the AS-IC imprinting defect could be achieved by mutations of *Arid4a*, *Arid4b*, or *Rb*. All mice with only the AS-IC^{an} mutation (total 15 mice in Fig. 6B–D and ~50 mice in the previous publication; Wu et al. 2006) had absence of methylation at *Snrpn*. The null hypothesis is that all mice (100%) with the AS-IC^{an} mutation should show an abnormal unmethylated pattern at *Snrpn*, and that any deviations from the 100% rate could be considered significant. We showed the corrected differential methylation pattern in mice with the AS-IC^{an} mutation when together with the *Arid4b* (five out of 12 mice in Fig. 6B), *Arid4a* (four out of 18 mice in Fig. 6C), or *Rb* (three out of 10 mice in Fig. 6D) mutations. In Figure 7, we showed the corrected differential methylation pattern in all mice with the AS-IC mutation when both parents carry the *Arid4a* mutation. This suppression of the AS-IC imprinting defect also associated with relieving the repression of *Ube3a*.

Inactivation of *RB* is seen in many human tumors. RB has been shown to be involved in many cellular processes, such as control of the cell cycle, cell differentiation, DNA-damage responses, DNA replication, and protection against apoptosis, all of which could contribute to the role of RB as a tumor suppressor (Classon and Harlow 2002). ARID4A and ARID4B may be directly related to key aspects of cell transformation, and represent biologically plausible candidate genes for involvement in breast cancer (Cao et al. 1999, 2001; Takahashi et al. 1999). Loss of imprinting has been reported in several types of human tumors (Feinberg et al. 2002). There is very little information about the presence or absence of imprinting defects in retinoblastoma, but one report suggested abnormal imprinting in RB tumors (Kato et al. 1996). Our evidence that *Rb*, *Arid4a*, and *Arid4b* can regulate genomic imprinting raises the question of whether dysfunction of the RB/ARID4A/ARID4B complex could disrupt genomic imprinting and/or epigenetic regulation and thereby promote tumor formation. This can be tested in human and mouse tumors lacking these proteins or in tissues and cultured cells from mice with conditional mutations.

Epigenetics refers to mechanisms for gene regulation by modifications of the DNA–protein complexes that are stable within a cell but do not involve a change in DNA sequence, and genomic imprinting is a subset of epigenetics. In this report, we identified *Arid4a* and *Arid4b* as new members of epigenetic regulatory complexes that control the Prader-Willi/Angelman imprinted domain. We believe that the role of epigenetics is neglected as a potential disease mechanism in conditions other than cancer, particularly in complex disease traits (Jiang et al. 2004). It will be of interest to determine whether mutations in *ARID4A* and *ARID4B* genes could contribute to epigenetic mechanisms of human disease.

Materials and methods

Targeting vectors

To construct the targeting vector for the *Snrpn*-EGFP fusion gene, a promoterless EGFP gene was removed from plasmid pIRES-EGFP (BD Bioscience Clontech), and was introduced upstream of the neomycin expression cassette flanked by loxP sites. The targeting vector included the 5′-homologous arm and 3′-homologous arm (Tsai et al. 2002) flanking the EGFP and neomycin cassettes, and there was an HSV-TK expression cassette outside the 3′-homologous region. To target the *Arid4a* and *Arid4b* loci, we isolated overlapping λ phage clones from a 129/SvEv genomic library. We constructed a targeting vector designed to delete a part of exons 1 and 2 in *Arid4a* by cloning a 2.7-kb EcoRI–XhoI phage clone end fragment as the 5′-homologous arm and a 4.1-kb XhoI phage clone end fragment as the 3′-homologous arm. The targeting vector included the 5′-homologous arm and the 3′-homologous arm flanking LacZ and neomycin cassettes; there was an HSV-TK expression cassette outside the 5′-homologous region. The *Arid4b* targeting vector was designed to delete 5.5 kb surrounding exon 1 by cloning a 3.1-kb SalI phage clone end fragment as the 5′-homologous arm and a 3.4-kb HindIII–EcoRI phage clone end fragment as the 3′-homologous arm. The targeting vector included the 5′- and 3′-homologous arms flanking the neomycin cassette; there was an HSV-TK expression cassette outside the 3′-homologous region.

Generation of mice with Arid4a and Arid4b deletions

The targeting vector for *Arid4a* or *Arid4b* deletion was electroporated into AB2.2 ES cells from the 129/SvEv strain provided by Allan Bradley (The Wellcome Trust Sanger Institute, Hinxton, Cambridge, UK). Neomycin (G418 sulfate, 200 mg/mL; Life

Technologies) was used to select for ES cells undergoing the desired recombination event. DNA extracted from ES cells was analyzed either by Southern blot hybridization using 5′-flanking and 3′-flanking probes, or by PCR amplification using primers as follows: primer a, 5′-GCTACAGAGTGATTTTATGCTG TC-3′; primer b, 5′-CACACTAGTCATAACTATGCTTTGTG-3′; and primer c, 5′-CCTGACTAGGGGAGGAGTAGAAG-3′. The targeted clones were injected into C57BL6/J blastocysts and reimplanted into pseudopregnant female mice. Chimeric males were bred to C57BL6/J females to evaluate germline transmission, and both mutations were maintained on a hybrid C57BL6/J and 129/SvEv genetic background.

Southern blot analysis

The targeted ES clones with the *Snrpn*-EGFP fusion gene were identified by Southern blot hybridization using a 2-kb PCR fragment as a 3′-flanking probe after DNA extracted from ES cells was digested with PstI. For disrupting the *Arid4a* gene, the targeted ES clones were identified by Southern blot analysis using a 1.7-kb PCR fragment as a 5′-flanking probe after genomic DNA was digested with EcoRI and a 660-bp PCR fragment as a 3′-flanking probe after genomic DNA was digested with NcoI. For disrupting the *Arid4b* gene, the targeted ES clones were identified by Southern blot analysis using a 360-bp PCR fragment as a 5′-flanking probe after DNA extracted from ES cells was digested with SstI. Southern blots prepared for differential methylation analyses at the *Snrpn* and *Ndn* loci were hybridized with a 1.3-kb BssHII–EcoRI fragment from *Snrpn* intron 1 or a 1.5-kb SacI–HindIII fragment from the *Ndn* 5′-flanking region after genomic DNA isolated from tail biopsies was digested with HindIII alone or in combination with SacII as described (Bressler et al. 2001).

RT–PCR analysis

RNA from the gene trap clone was isolated using Trizol Reagent (Invitrogen) according to the manufacturer's directions. RT–PCR amplification was performed using SuperScript one-step RT–PCR (Invitrogen). The *Arid4a* transcripts were analyzed using the primer as follows: primer e1, 5′-ATGAAGGCGGCA GATGAGCC-3′ and primer e5, 5′-CACAGTATACCAACTT GCATCTG-3′. *Hprt* transcripts were amplified using the primer pair 5′-ATGACCTAGATTTGTTTTGTATACC-3′ and 5′-GTAGCTCTTCAGTCTGATAAAATCTAC-3′. For quantitative RT–PCR analysis, reverse transcription was performed using random hexamers to primer the first-strand cDNA synthesis using DNase I-treated (Promega) total RNA and the SuperScript First-Strand Synthesis System (Invitrogen). Quantitative RT–PCR analysis was performed using LightCycler Fast-Start DNA Master SYBR Green I (Roche). The sequences of PCR primers for *Snrpn* exon 2 and *Ndn* were as described (Yang et al. 1998; Tsai et al. 1999).

ChIP assay

We electroporated the expression vector Flag-ARID4A into AB2.2 ES cells followed by selection with 200 mg/mL Geneticin for 10 d. A stable clone expressing Flag-ARID4A protein was isolated and used to carry out ChIP assays with anti-Flag M2 antibody (Sigma) as described by the protocol of Upstate Biotechnology (available at http://www.upstate.com). For chromatin modification analysis, chromatin extracted from murine brain was immunoprecipitated with anti-trimeH3K9 and anti-trimeH4K20 antibodies (Upstate Biotechnology). The primer sets used to amplify the *Snrpn* gene were as follows: primer pair 1, 5′-CTGGCCACCAGTAACTAAATAAC-3′ (forward) and 5′-GTGTGACTTGAACATTGAAGGCC-3′ (reverse); primer pair 2, 5′-CTGTGTAGCACTGGCTAACCTG-3′ (forward) and 5′-GAGTCTAGTCTGATCTACAGAGTG-3′ (reverse); primer pair 3, 5′-GTCACACAGCATCCCAATTTCTTC-3′ (forward) and 5′-CAGGTAAATTCTTACCACGTGGC-3′ (reverse); primer pair e1, 5′-GAGTGATTTGCAACGCAATGGAGCG-3′ (forward) and 5′-CTAACACACCCAAGGAGTCCGTCTG-3′ (reverse); primer pair 4, 5′-CAAGTCAGAGAAGTGATTGTG TG-3′ (forward) and 5′-GTCTGGCCATTCTACACAGGT TC-3′ (reverse); primer pair e3, 5′-AGGAGGCTCTTTTAGAG TAAAGGTG-3′ (forward) and 5′-CACCACCTTGAAGTTG CAATACTGC-3′ (reverse); primer pair e7, 5′-ACTGGCATT GCTCGTGTGCCTC-3′ (forward) and 5′-GCCTCCAACTG CTCGGACAGG-3′ (reverse).

Cloning of cDNA

Arid4b-βgeo and *Arid4a*-βgeo fusion cDNAs were amplified by the 5′-RACE system (Life Technologies). We used three β-gal gene-specific primers (GSP) as follows: GSP1, 5′-GCCATCA AAAATAATTCGCGTCT-3′; GSP2, 5′-CGTTGGTGTAGAT GGGCGCATCGT-3′; and GSP3, 5′-CGTGCATCTGCCAG TTTGAGG-3′. The *Arid4b* transcripts were analyzed using the primer as follows: primer e1, 5′-GGTGCAGGTGAAGCTGGT GTC-3′ and primer e3, 5′-CACAGTATACCAACTTGCAT CTG-3′. To generate the vector expressing Flag-hARID4A, the coding region from a full-length human *ARID4A* cDNA clone (ATCC no. 95680) was cloned into the pCMV-Tag2 plasmid (Stratagene) with a Flag epitope in frame at the N terminus. A mouse *Arid4b* EST clone (Invitrogen; clone ID: 3970761) was used to screen a mouse brain cDNA library (BD Bioscience Clontech). A clone was isolated and used in combination with two mouse EST clones (Invitrogen; clone ID: 3970761 and 3603654) to construct an expression cassette containing further 5′ and 3′ sequences, respectively. The full-length mouse *Arid4b* cDNA was tagged at the C-terminal with a V5 epitope in the expression vector pcDNA3.1/V5-His B (Invitrogen).

Immunoprecipitation and Western blotting

Human embryonic kidney 293 cells were transfected using LipofectAMINE (Invitrogen). Whole-cell extracts were prepared in lysis buffer (50 mM Tris at pH 8.0, 200 mM NaCl, 0.5% [v/v] Nonidet P-40, 100 mM NaF, 0.2 mM sodium orthovanadate, and protease inhibitors [Roche]), and subjected to immunoprecipitation and Western blotting with antibodies (anti-Flag M2 antibody [Sigma], anti-V5 antibody [Invitrogen], anti-ARID4A antibody [Upstate Biotechnology, anti-RBBP1 clone LY11], or normal mouse IgG [Upstate Biotechnology]). Western blot analysis for *Ube3a* expression used anti-E6AP antibody (Bethyl; BL447) as described (Wu et al. 2006).

Bisulfite sequencing analysis

Bisulfite treatment of genomic DNA was carried out using the EZ DNA methylation-gold kit (ZYMO Research). Bisulfite-modified DNA was amplified by nested PCR as described (Wu et al. 2006).

Acknowledgments

We thank Silvia Briones, Monica Lee, Catherine Tran, and Minnie Freeman for technical assistance. This work was supported by NIH grant HD37283 to A.L.B.

References

Bannister, A.J. and Kouzarides, T. 2005. Reversing histone methylation. *Nature* **436:** 1103–1106.

Bannister, A.J., Zegerman, P., Partridge, J.F., Miska, E.A., Thomas, J.O., Allshire, R.C., and Kouzarides, T. 2001. Selective recognition of methylated lysine 9 on histone H3 by the HP1 chromo domain. *Nature* **410:** 120–124.

Bressler, J., Tsai, T.F., Wu, M.Y., Tsai, S.F., Ramirez, M.A., Armstrong, D., and Beaudet, A.L. 2001. The SNRPN promoter is not required for genomic imprinting of the Prader-Willi/Angelman domain in mice. *Nat. Genet.* **28:** 232–240.

Buiting, K., Saitoh, S., Gross, S., Dittrich, B., Schwartz, S., Nicholls, R.D., and Horsthemke, B. 1995. Inherited microdeletions in the Angelman and Prader-Willi syndromes define an imprinting centre on human chromosome 15. *Nat. Genet.* **9:** 395–400.

Buiting, K., Lich, C., Cottrell, S., Barnicoat, A., and Horsthemke, B. 1999. A 5-kb imprinting center deletion in a family with Angelman syndrome reduces the shortest region of deletion overlap to 880 bp. *Hum. Genet.* **105:** 665–666.

Cao, J., Gao, T., Giuliano, A.E., and Irie, R.F. 1999. Recognition of an epitope of a breast cancer antigen by human antibody. *Breast Cancer Res. Treat.* **53:** 279–290.

Cao, J., Gao, T., Stanbridge, E.J., and Irie, R. 2001. RBP1L1, a retinoblastoma-binding protein-related gene encoding an antigenic epitope abundantly expressed in human carcinomas and normal testis. *J. Natl. Cancer Inst.* **93:** 1159–1165.

Classon, M. and Harlow, E. 2002. The retinoblastoma tumour suppressor in development and cancer. *Nat. Rev. Cancer* **2:** 910–917.

Defeo-Jones, D., Huang, P.S., Jones, R.E., Haskell, K.M., Vuocolo, G.A., Hanobik, M.G., Huber, H.E., and Oliff, A. 1991. Cloning of cDNAs for cellular proteins that bind to the retinoblastoma gene product. *Nature* **352:** 251–254.

Feinberg, A.P., Cui, H., and Ohlsson, R. 2002. DNA methylation and genomic imprinting: Insights from cancer into epigenetic mechanisms. *Semin. Cancer Biol.* **12:** 389–398.

Fleischer, T.C., Yun, U.J., and Ayer, D.E. 2003. Identification and characterization of three new components of the mSin3A corepressor complex. *Mol. Cell. Biol.* **23:** 3456–3467.

Fournier, C., Goto, Y., Ballestar, E., Delaval, K., Hever, A.M., Esteller, M., and Feil, R. 2002. Allele-specific histone lysine methylation marks regulatory regions at imprinted mouse genes. *EMBO J.* **21:** 6560–6570.

Friedrich, G. and Soriano, P. 1991. Promoter traps in embryonic stem cells: A genetic screen to identify and mutate developmental genes in mice. *Genes & Dev.* **5:** 1513–1523.

Fulmer-Smentek, S.B. and Francke, U. 2001. Association of acetylated histones with paternally expressed genes in the Prader-Willi deletion region. *Hum. Mol. Genet.* **10:** 645–652.

Gabriel, J.M., Gray, T.A., Stubbs, L., Saitoh, S., Ohta, T., and Nicholls, R.D. 1998. Structure and function correlations at the imprinted mouse Snrpn locus. *Mamm. Genome* **9:** 788–793.

Gonzalo, S., Garcia-Cao, M., Fraga, M.F., Schotta, G., Peters, A.H., Cotter, S.E., Eguia, R., Dean, D.C., Esteller, M., Jenuwein, T., et al. 2005. Role of the RB1 family in stabilizing histone methylation at constitutive heterochromatin. *Nat. Cell Biol.* **7:** 420–428.

Horsthemke, B. and Buiting, K. 2006. Imprinting defects on human chromosome 15. *Cytogenet. Genome Res.* **113:** 292–299.

Jiang, Y.H., Bressler, J., and Beaudet, A.L. 2004. Epigenetics and human disease. *Annu. Rev. Genomics Hum. Genet.* **5:** 479–510.

Kantor, B., Shemer, R., and Razin, A. 2006. The Prader-Willi/Angelman imprinted domain and its control center. *Cytogenet. Genome Res.* **113:** 300–305.

Kato, M.V., Shimizu, T., Nagayoshi, M., Kaneko, A., Sasaki, M.S., and Ikawa, Y. 1996. Genomic imprinting of the human serotonin-receptor (HTR2) gene involved in development of retinoblastoma. *Am. J. Hum. Genet.* **59:** 1084–1090.

Lachner, M., O'Carroll, D., Rea, S., Mechtler, K., and Jenuwein, T. 2001. Methylation of histone H3 lysine 9 creates a binding site for HP1 proteins. *Nature* **410:** 116–120.

Lai, A., Lee, J.M., Yang, W.M., DeCaprio, J.A., Kaelin Jr., W.G., Seto, E., and Branton, P.E. 1999a. RBP1 recruits both histone deacetylase-dependent and -independent repression activities to retinoblastoma family proteins. *Mol. Cell. Biol.* **19:** 6632–6641.

Lai, A., Marcellus, R.C., Corbeil, H.B., and Branton, P.E. 1999b. RBP1 induces growth arrest by repression of E2F-dependent transcription. *Oncogene* **18:** 2091–2100.

Lai, A., Kennedy, B.K., Barbie, D.A., Bertos, N.R., Yang, X.J., Theberge, M.C., Tsai, S.C., Seto, E., Zhang, Y., Kuzmichev, A., et al. 2001. RBP1 recruits the mSIN3-histone deacetylase complex to the pocket of retinoblastoma tumor suppressor family proteins found in limited discrete regions of the nucleus at growth arrest. *Mol. Cell. Biol.* **21:** 2918–2932.

Lee, E.Y., Chang, C.Y., Hu, N., Wang, Y.C., Lai, C.C., Herrup, K., Lee, W.H., and Bradley, A. 1992. Mice deficient for Rb are nonviable and show defects in neurogenesis and haematopoiesis. *Nature* **359:** 288–294.

Nielsen, S.J., Schneider, R., Bauer, U.M., Bannister, A.J., Morrison, A., O'Carroll, D., Firestein, R., Cleary, M., Jenuwein, T., Herrera, R.E., et al. 2001. Rb targets histone H3 methylation and HP1 to promoters. *Nature* **412:** 561–565.

Ohta, T., Gray, T.A., Rogan, P.K., Buiting, K., Gabriel, J.M., Saitoh, S., Muralidhar, B., Bilienska, B., Krajewska-Walasek, M., Driscoll, D.J., et al. 1999. Imprinting-mutation mechanisms in Prader-Willi syndrome. *Am. J. Hum. Genet.* **64:** 397–413.

Patsialou, A., Wilsker, D., and Moran, E. 2005. DNA-binding properties of ARID family proteins. *Nucleic Acids Res.* **33:** 66–80.

Perk, J., Makedonski, K., Lande, L., Cedar, H., Razin, A., and Shemer, R. 2002. The imprinting mechanism of the Prader-Willi/Angelman regional control center. *EMBO J.* **21:** 5807–5814.

Quina, A.S., Buschbeck, M., and Di Croce, L. 2006. Chromatin structure and epigenetics. *Biochem. Pharmacol.* doi:10.1016/j.bcp.2006.06.016.

Saitoh, S. and Wada, T. 2000. Parent-of-origin specific histone acetylation and reactivation of a key imprinted gene locus in Prader-Willi syndrome. *Am. J. Hum. Genet.* **66:** 1958–1962.

Sanders, S.L., Portoso, M., Mata, J., Bahler, J., Allshire, R.C., and Kouzarides, T. 2004. Methylation of histone H4 lysine 20 controls recruitment of Crb2 to sites of DNA damage. *Cell* **119:** 603–614.

Shemer, R., Birger, Y., Riggs, A.D., and Razin, A. 1997. Structure of the imprinted mouse Snrpn gene and establishment of its parental-specific methylation pattern. *Proc. Natl. Acad. Sci.* **94:** 10267–10272.

Takahashi, T., Cao, J., Hoon, D.S., and Irie, R.F. 1999. Cytotoxic T lymphocytes that recognize decameric peptide sequences of retinoblastoma binding protein 1 (RBP-1) associated with human breast cancer. *Br. J. Cancer* **81:** 342–349.

Tsai, T.F., Jiang, Y.H., Bressler, J., Armstrong, D., and Beaudet, A.L. 1999. Paternal deletion from Snrpn to Ube3a in the mouse causes hypotonia, growth retardation and partial lethality and provides evidence for a gene contributing to

Prader-Willi syndrome. *Hum. Mol. Genet.* **8:** 1357–1364.
Tsai, T.F., Chen, K.S., Weber, J.S., Justice, M.J., and Beaudet, A.L. 2002. Evidence for translational regulation of the imprinted Snurf-Snrpn locus in mice. *Hum. Mol. Genet.* **11:** 1659–1668.
Tsai, T.F., Bressler, J., Jiang, Y.H., and Beaudet, A.L. 2003. Disruption of the genomic imprint in *trans* with homologous recombination at Snrpn in ES cells. *Genesis* **37:** 151–161.
Wilsker, D., Probst, L., Wain, H.M., Maltais, L., Tucker, P.W., and Moran, E. 2005. Nomenclature of the ARID family of DNA-binding proteins. *Genomics* **86:** 242–251.
Wu, M.Y., Chen, K.S., Bressler, J., Hou, A., Tsai, T.F., and Beaudet, A.L. 2006. Mouse imprinting defect mutations that model Angelman syndrome. *Genesis* **44:** 12–22.
Xin, Z., Allis, C.D., and Wagstaff, J. 2001. Parent-specific complementary patterns of histone H3 lysine 9 and H3 lysine 4 methylation at the Prader-Willi syndrome imprinting center. *Am. J. Hum. Genet.* **69:** 1389–1394.
Yang, T., Adamson, T.E., Resnick, J.L., Leff, S., Wevrick, R., Francke, U., Jenkins, N.A., Copeland, N.G., and Brannan, C.I. 1998. A mouse model for Prader-Willi syndrome imprinting-centre mutations. *Nat. Genet.* **19:** 25–31.
Zhu, L. 2005. Tumour suppressor retinoblastoma protein Rb: A transcriptional regulator. *Eur. J. Cancer* **41:** 2415–2427.